Journal of Physics: Condensed Matter

PERSPECTIVE

Ferromagnetic ferroelectricity due to orbital ordering

I V Solovyev*

Research Center for Materials Nanoarchitectonics (MANA), National Institute for Materials Science (NIMS), 1-1 Namiki, Tsukuba, Ibaraki 305-0044, Japan

* Author to whom any correspondence should be addressed.

E-mail: SOLOVYEV.Igor@nims.go.jp

Keywords: ferroelectricity, ferromagnetism, orbital ordering, Hund's rules

OPEN ACCESS

RECEIVED
2 February 2026

REVISED
23 March 2026

ACCEPTED FOR PUBLICATION
10 April 2026

PUBLISHED
20 April 2026

Abstract

Realization of ferromagnetic (FM) ferroelectricity, combining two ferroic orders in a single phase, is the longstanding problem of great practical importance. One of the difficulties is that ferromagnetism alone cannot break the inversion symmetry $\mathcal{I}$. Therefore, such a phase cannon be obtained by purely magnetic means, as in other multiferroics with complex magnetic order. Here, we show how it can be designed by considering orbital degrees of freedom. The idea can be traced back to a basic principle of interatomic exchange coupling, which states that an alternation of occupied orbitals along a bond (i.e. antiferro orbital order) favors FM interactions between the spins. The new aspect of this canonical picture is that the antiferro orbital order breaks $\mathcal{I}$, so that the bond becomes not only FM but also ferroelectric (FE). Then, we formulate basic principles governing the realization of such a state in solids, namely: (i) the magnetic atoms should not be located in inversion centers, as in the honeycomb lattice; (ii) the orbitals should be flexible enough to change they shape and minimize the energy of exchange interactions; (iii) this flexibility can be achieved by intraatomic interactions, which are responsible for Hund's second rule and compete with the crystal field splitting; (iv) for octahedrally coordinated transition-metal compounds, the most promising candidates are iodides with a d^2 configuration and relatively weak d–p hybridization. The situation is illustrated on the van der Walls compound VI_3, which we expect to be FM FE.

1. Introduction

Multiferroicity means a coexistence of two or more ferroic orders within one phase. Thus, literally, it should be a combination of *ferro*magnetism, *ferro*electricity, *ferro*elasticity, or any other property with the prefix *ferro*. Such a combination is of great practical importance: Because these ferroic properties are intertwined, multiferroics offer an excellent platform for cross-control of polarization by the magnetic field and magnetization by the electric field [1]. The prefix *ferro* appears to be very important also in the practical context: the larger the magnetization (polarization), the weaker the magnetic (electric) field needed to achieve this cross-control.

However, today the term multiferroicity is understood in a more general sense, when ferroelectricity coexists with *any* type of magnetic order and not necessarily the ferromagnetic (FM) one [2–4], while FM ferroelectrics (FEs) are very rare [5].

FM ferroelectricity is expected in materials with two or more sublattices, where one sublattice hosts ferromagnetism and another ferroelectricity [6, 7]. Typically, these ferroic properties have different microscopic origin and only weakly depend on each other. A notable exception is $SrMnO_3$ under epitaxial strain, which was predicted to be simultaneously FM and FE, and both of these properties stem from the Mn sublattice [8, 9]. Another possibility is the synthesis of artificial heterostructures, combining layers of FM and FE materials [10].

A new route for realizing FM ferroelectricity has been proposed in [11]. The basic idea is traced back to Goodenough–Kanamori–Anderson (GKA) rules for interatomic exchange interactions [12–15], which state basically that population of alike orbitals at two sites of the bond (the ferro orbital order) favors antiferromagnetic (AFM) coupling, while population of unlike orbitals (the antiferro orbital order) will

make this coupling FM. Nevertheless, what was overlooked in the canonical GKA picture is that, besides FM coupling, the antiferro orbital order breaks the inversion symmetry $\mathcal{I}$ in the bond so that it becomes simultaneously FM and FE. The idea was further adapted for periodic solids, arguing that in certain materials the spontaneous antiferro orbital order can yield the FM-FE state. The van der Walls FM semiconductor VI_3 is one of potential candidates for realizing such a state [11, 16].

In this article, we further elaborate the basic conditions and perspectives of realizing the orbitally induced FM-FE state in real materials. After reminding in section 2 key results of the modern theory of electric polarization, in section 3 we will consider possible mechanisms of inversion symmetry breaking in solids. The main conclusion is that the FM-FE state cannot be realized by magnetic means alone: the FM order is too simple to break $\mathcal{I}$. Then, in section 4, we will turn to the orbital degrees of freedom and show how, by populating different combinations of orbitals at two sites of the bond, one can control not only the exchange coupling but also the electric polarization in the bond. Thus, the orbital degrees of freedom appear to be that additional ingredient, which can help us in realizing the FM-FE state. In section 5, we will turn to more practical aspects and consider the conditions, which should be met in order to realize the FM-FE state in solids: type of the lattice, electronic configuration of magnetic ions, type of the ligand atoms, details of the electronic structure, etc. Particularly, the antiferro orbital order can be obtained by minimizing the energy of exchange interactions [17–19], meaning that occupied orbitals should be flexible enough to change their shape depending on the spin coupling. This flexibility can be achieved by intraatomic interactions responsible for Hund's second rule, which forces the atomic ground state to have maximal orbital degeneracy and competes with the Jahn–Teller (JT) distortion, acting in the opposite direction and tending to freeze occupied orbitals in one particular configuration. Then, in section 6, we discuss results of numerical simulations for VI_3, using for these purposes realistic model derived from first-principle electronic structure calculations. Finally, in section 7, we summarize our material design strategy for FM FEs and discuss possible implications of the Hund's physics to the properties of magnetic materials.

2. Theoretical background

In quantum mechanics, the electric polarization is given by the expectation value of the position operator $\vec{r}$:

$$\vec{P} = -\frac{e}{V}\langle\Psi\,|\vec{r}|\,\Psi\rangle,$$

where $-e$ is the electron charge, V is the volume, and Ψ is the ground state wavefunction. Since $\mathcal{I}$ transforms the polar vector $\vec{r}$ to $-\vec{r}$, the spontaneous polarization can develop only when $\mathcal{I}$ is macroscopically broken. In this sense, the search of new types of FE materials is essentially the search of new possibilities how to break $\mathcal{I}$. Some of such possibilities will be briefly reviewed in section 3.

According to the modern theory of electric polarization in periodic systems [20, 21], $\vec{P}$ can be computed either in the k-space, via the Berry connection:

$$\vec{P} = -\frac{ie}{(2\pi)^3}\sum_{n=1}^{M}\int_{\rm BZ}\langle n\vec{k}|\vec{\nabla}_{\vec{k}}|n\vec{k}\rangle\,{\rm d}\vec{k}, \tag{1}$$

or, equivalently, in the r-space, via the Wannier functions w_n for the occupied states:

$$\vec{P} = -\frac{e}{V}\sum_{n=1}^{M}\int\vec{r}\,|w_n(\vec{r})|^2{\rm d}\vec{r}. \tag{2}$$

The latter expression is especially important for understanding microscopic origin of magnetoelectric coupling. Since $\vec{r}$ does not depend on spin degrees of freedom, all information about magnetic state dependence of $\vec{P}$ is accumulated in w_n. Equation (2) is also useful for finding the analytical dependence of $\vec{P}$ on the magnetization in the framework of superexchange theory [22–24].

3. Mechanisms of inversion symmetry breaking

3.1. Hybridization between bonding and antibonding states

The first canonical example of FE materials is the so-called d^0 perovskites, which include such representative compounds as $BaTiO_3$ and $KNbO_3$ [25]. From the viewpoint of electronic structure in paraelectric

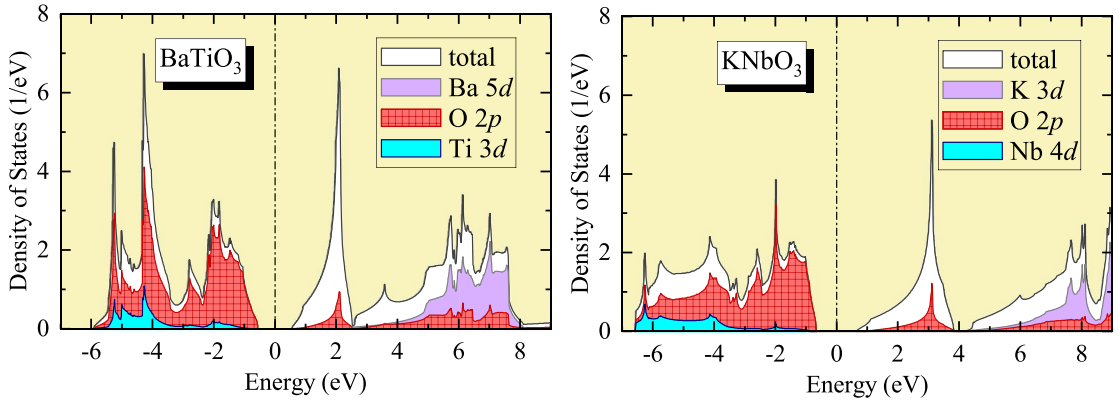

Figure 1. Total and partial densities of states of cubic $BaTiO_3$ and $KNbO_3$ in the local density approximation. The Fermi level is in the middle of the band gap (shown by dot-dashed line).

cubic phase, the key aspect of these materials is the strong hybridization between the transition-metal d and oxygen p states, which splits them around the Fermi level, forming the bonding O $2p$ band and antibonding Ti $3d$ or Nb $4d$ band (figure 1). Because of this hybridization, both materials are insulators. Moreover, the bonding and antibonding states can be viewed as, respectively, symmetric and antisymmetric states relative to some inversion center. Then, the polar distortion, δQ, mixing these symmetric and antisymmetric states, will additionally shift the occupied O $2p$ band to the lower energy region, giving a possibility to realize the FE phase with spontaneously broken $\mathcal{I}$. This mechanism was proposed long ago by Bersuker using model considerations [26]. A transparent illustration was give by Cohen on the basis of first-principles electronic structure calculations [27].

The corresponding energy gain is even in δQ. This is different from the conventional JT effect, which splits the degenerate states and, therefore, is odd in δQ [28]. To emphasize this difference, the mechanism is called *pseudo* JT effect. Then, the electronic energy gain should be combined with the energy loss, $\sim(\delta Q)^2$, resulting from the harmonic ion core motion [25]. Depending on parameters, the total energy can have a minimum at finite δQ, signaling that the FE phase is stable and $\mathcal{I}$ is broken.

However, the d^0 perovskites are intrinsically nonmagnetic. The magnetism would require a partial population of antibonding transition-metal band. Therefore, it will reduce the energy gain caused by mixing of bonding and antibonding bands, that will act against the instability towards the FE state. Nevertheless, certain populations of transition-metal states may still lead to the FE instability [29] and according to the first-principles calculations the FM ferroelectricity can be indeed realized in the d^3 compound $SrMnO_3$ under epitaxial strain [8, 9].

Another important ingredient is the lone pair $6s^2$ electrons residing on the A sites of such perovskites as $PbTiO_3$ and $BiMnO_3$ [6]. The off-centrosymmetric displacements of A sites induce the hybridization of the occupied $6s^2$ states with unoccupied states of opposite parity, which additionally stabilizes the polar phase.

3.2. Type-II multiferroicity

$\mathcal{I}$ can be broken by magnetic order. Such materials are called type-II multiferroics [3]. The canonical examples are spin-spiral insulators, where the onset of conical or cycloidal magnetic order gives rise to spontaneous polarization [30, 31].

Thus, one can have a unique combination of ferroelectricity and magnetism, which can be used to mutually control each other applying either electric or magnetic field [1]. However, literally, the multiferroicity means something different. It implies the combination of several *ferroic* orders, so that the material should be not simply magnetic, but FM. Therefore, the next question is: Can the FM order alone break the inversion symmetry?

To answer this question, one should understand why certain magnetic textures break $\mathcal{I}$. To be specific, let us consider the centrosymmetric bond connecting two noncollinear spins. This bond can be regarded as a part of cycloidal texture (figure 2). Then, the noncollinear configuration of spins in the bonds can be presented as the superposition of collinear FM and AFM counterparts [24]. While the FM configuration is transformed to itself by $\mathcal{I}$ about the bond center, the AFM configuration is transformed

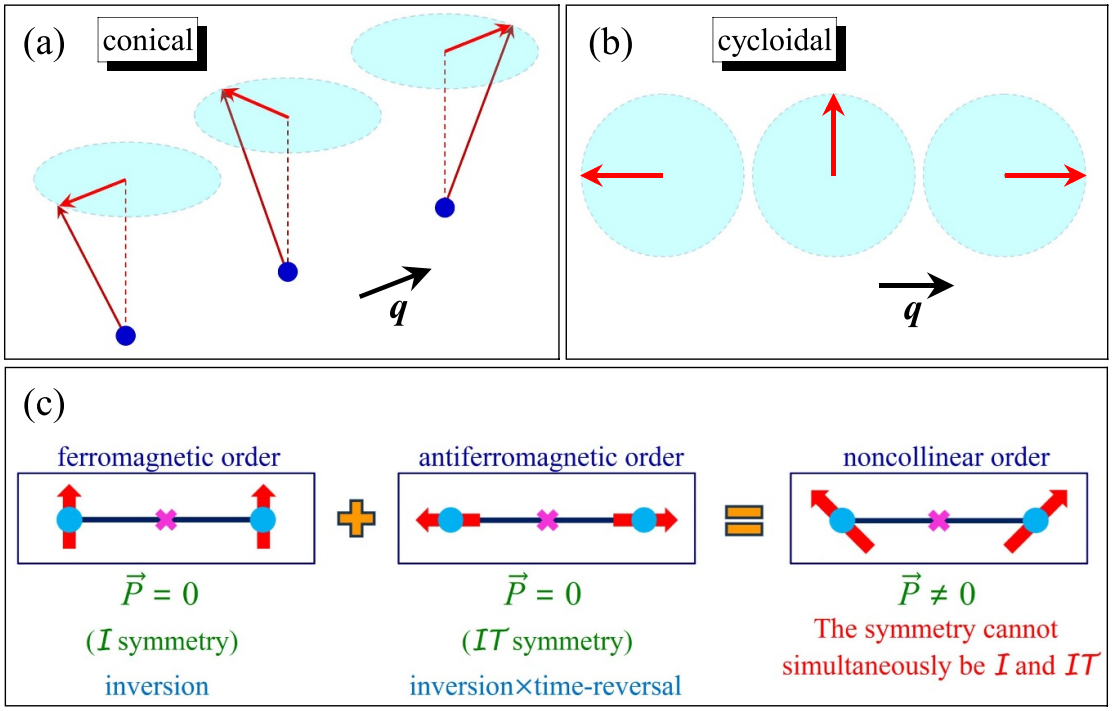

Figure 2. Spin spirals and inversion symmetry breaking. (a) Conical and (b) cycloidal magnetic order. $\boldsymbol{q}$ is the propagation vector. (c) Illustration of inversion symmetry breaking by noncollinear spins in centrosymmetric bond. × is the inversion center. The noncollinear spin configuration can be decomposed in ferromagnetic and antiferromagnetic counterparts. The former is invariant under $\mathcal{I}$, while the latter is invariant under $\mathcal{IT}$. Since $\mathcal{I}$ cannot coexist with $\mathcal{IT}$, the inversion symmetry is broken. Reproduced from [24]. CC BY 4.0.

to itself by $\mathcal{IT}$, where $\mathcal{I}$ is combined with the time reversal $\mathcal{T}$, which additionally flips the spins[1]. However, $\mathcal{I}$ cannot coexist with $\mathcal{IT}$ because otherwise $\mathcal{T} \equiv \mathcal{IIT}$ would be another symmetry operation and the system would become nonmagnetic. The only possibility to resolve this conflict between FM and AFM counterparts coexisting in the noncollinear texture of spins is to break $\mathcal{I}$ [24]. This is the phenomenological reason why spiral magnetic order can induce the electric polarization. The microscopic explanation was proposed by Katsura, Nagaosa, and Balatsky [32] and refined later in the series of publications [23, 24, 33, 34].

The rule is generic and applies not only to spin-spiral compounds but to all type-II multiferroics. In all these materials, the magnetic texture should involve simultaneously FM and AFM counterparts, transforming via, respectively, $\mathcal{I}$ and $\mathcal{IT}$ [24]. Therefore, the answer to the above question is *no*: the FM order is just too simple to break the inversion symmetry.

4. Orbital degrees of freedom

Thus, the conventional type-II multiferroics cannot be FM: in order to break $\mathcal{I}$ by spin degrees of freedom, it is necessary to destroy the ferromagnetism. This means that in order to achieve the FM-FE state, it is essential to consider additional degrees of freedom, which would control the magnetic coupling in the bonds *and* simultaneously break $\mathcal{I}$. Below, we explore the potential of orbital degrees of freedom, which play a very important role in magnetism.

4.1. GKA rules and local breaking of inversion symmetry

There are five *d* orbitals and the magnetic properties of solids strongly depend on which orbitals are occupied and which are empty, and how the occupied orbitals are aligned relative to each other. The canonical example is the phenomenological GKA rules, proposed back in the 1950s [12–15].

These rules state essentially that if electrons occupy the same orbitals at two sites of the bond (the so-called ferro orbital order), the exchange coupling will be AFM (figure 3).If they occupy different

[1] Note $\mathcal{I}$ does not change the direction of spin, which is the axial vector.

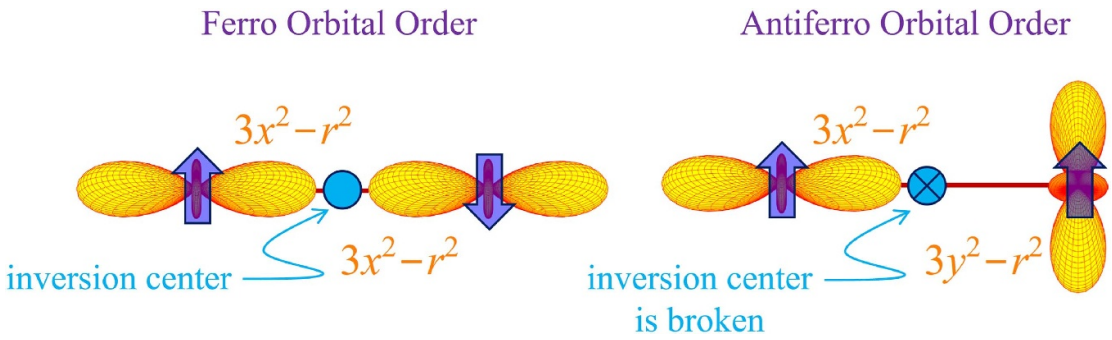

Figure 3. Examples of ferro and antiferro orbital order around the inversion center. Ferro orbital order tends to stabilize AFM coupling and preserve the inversion symmetry in the bond. Antiferro orbital order stabilizes FM coupling and breaks the inversion symmetry.

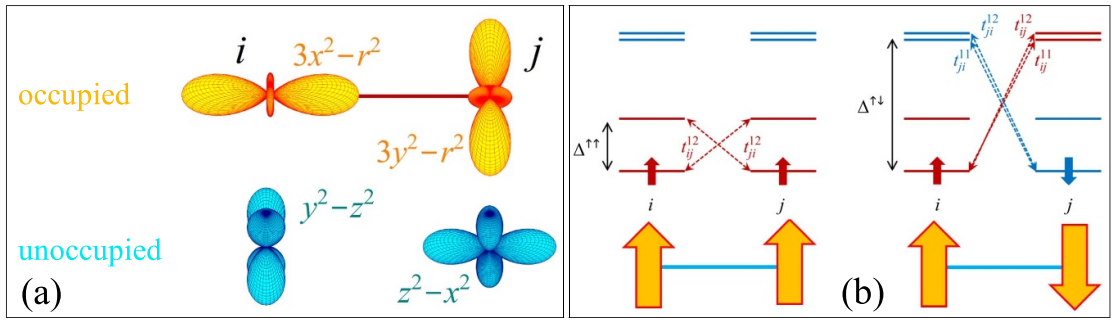

Figure 4. Illustration of superexchange interactions: (a) example of occupied and unoccupied orbitals in the bond; (b) transfer integrals between occupied and empty states in the case of FM and AFM alignment. The splitting is $\Delta^{\uparrow\uparrow} = U - J_{\rm H}/2 \equiv \tilde{U}$ and $\Delta^{\uparrow\downarrow} = U + J_{\rm H}/2$.

orbitals, aligned perpendicular to each other (antiferro orbital order), the exchange coupling will most likely be FM.

However, there is one important point, which was overlooked in this canonical GKA picture: the antiferro orbital order not only stabilizes the FM coupling but, since the occupied orbitals across the inversion center become inequivalent, also breaks $\mathcal{I}$ in the bond. Thus, at least in the single bond, one can easily realize the FM-FE state.

4.2. Superexchange theory

The superexchange theory provides the microscopic explanation for the GKA rules [35]. It starts with the atomic limit, where occupied and empty states are splits by the on-site Coulomb repulsion U and intraatomic exchange interaction $J_{\rm H}$, and treats transfer integrals between them as a perturbation. U in such a picture enforces the charge neutrality of the atomic configuration with the integer number of electrons, while $J_{\rm H}$ is responsible for Hund's first rule [36].

Then, the exchange coupling J_{ij} is obtained in the second-order perturbation theory for the energy difference between FM and AFM configurations in the bond. For instance, considering the superexchange processes involving the occupied $3x^2-r^2$ ($3y^2-r^2$) and unoccupied y^2-z^2 (z^2-x^2) e_g orbitals at the site i (j) (see figure 4), J_{ij} will be given by

$$J_{ij} = \frac{x\left[\left(t_{ij}^{12}\right)^2 + \left(t_{ji}^{12}\right)^2\right] - 2\left(t_{ij}^{11}\right)^2}{2\tilde{U}(1+x)},$$

where $t_{ij}^{11} = -1/2$, $t_{ij}^{12} = -\sqrt{3}/2$, and $t_{ji}^{12} = 0$ are the transfer integrals between occupied (1) and unoccupied (2) orbitals in terms of the two-center Slater–Koster integral $dd\sigma$ [37], $\tilde{U} = U - J_{\rm H}/2$, and

$x = J_H/\tilde{U}$[2]. Thus, the coupling is FM when $2J_H > U$. The tendency towards ferromagnetism is further enhanced if there are other d electrons, which tend to form high-spin state (due to J_H) and, therefore, favor the FM configuration when electrons transfer to neighboring sites with the same direction of spin. For instance, when beside e_g there are inner t_{2g} electrons, which interact via J_H, but do not participate in the hoppings processes, J_{ij} is described by the same equation but with $x = NJ_H/\tilde{U}$, where N is the total number of d electrons. Then, the FM coupling is stabilized when $\frac{3N+1}{2}J_H > U$. Such a situation is realized in perovskite manganites [38].

These are typical considerations for exchange interactions, which were known for decades. Nevertheless, similar arguments can be applied also to $\vec{P}$, starting from the expression (2) of the modern theory of electric polarization [20, 21]. Indeed, in the first-order perturbation theory, the occupied Wannier function at the site i will be given by

$$|w_i\rangle = |\alpha_i^1\rangle + \sum_{j\neq i} |\alpha_{i\to j}^1\rangle,$$

where α_i^1 is the 'head' residing at the central site i and $\alpha_{i\to j}^1$ are the 'tails' induced by the electron hoppings at the neighboring sites j. The latter can be evaluated using the perturbation theory as

$$|\alpha_{i\to j}^1\rangle = -\frac{t_{ij}^{12}}{\tilde{U}}|\alpha_j^2\rangle.$$

Then, assuming $\langle\alpha_i^a|\vec{r}|\alpha_j^b\rangle \approx \vec{R}_j\delta_{ij}\delta_{ab}$ [22] and using equation (2), it is straightforward to find the following expression for electric polarization in the bond ij:

$$\vec{P}_{ij} = \frac{e}{V}\frac{\left(t_{ij}^{12}\right)^2 - \left(t_{ji}^{12}\right)^2}{\tilde{U}^2}\left(\vec{R}_i - \vec{R}_j\right). \tag{3}$$

Thus, the polarization is finite if $t_{ij}^{12} \neq t_{ji}^{12}$, i.e. when the hoppings between occupied and empty orbitals are nonreciprocal. Such nonreciprocity is produced by the antiferro orbital order, which makes the directions $i \to j$ and $j \to i$ inequivalent.

4.3. Kugel–Khomskii theory

Kugel–Khomskii theory is basically a generalization of the superexchange theory, treating spin and orbital degrees of freedom on an equal footing [17–19]. If orbital degeneracy is lifted by the lattice distortion, deciding which orbitals are occupied and which are empty, it is reduced to the conventional superexchange theory, specifying the exchange coupling for the given configuration of occupied orbitals. In this case, the lattice distortion acts as an external constraining field in the spin–orbital (OS) system. However, if the lattice distortion is weak, there is certain element of self-organization, when the system decides the type of the orbital alignment by minimizing the energy of exchange interactions with respect to the orbital degrees of freedom for the given configuration of spins. If this orbital alignment appears to be of the antiferro type, it stabilizes the FM coupling and induces the electric polarization as described above.

The basic idea can be again illustrated by considering the superexchange processes between two e_g orbitals in the single bond oriented along x (see figure 4). If the e_g levels are degenerate, the occupied orbitals can be searched in the most general form, as a linear combination of the $|x^2 - y^2\rangle$ and $|3z^2 - r^2\rangle$ states:

$$|\alpha_i^1\rangle = \quad \cos\vartheta_i|x^2 - y^2\rangle + \sin\vartheta_i|3z^2 - r^2\rangle.$$

The unoccupied orbital is orthogonal to $|\alpha_i^1\rangle$:

$$|\alpha_i^2\rangle = -\sin\vartheta_i|x^2 - y^2\rangle + \cos\vartheta_i|3z^2 - r^2\rangle.$$

[2] The corresponding exchange energy in the bond is defined as $-J_{ij}\boldsymbol{e}_i \cdot \boldsymbol{e}_i$, where $\boldsymbol{e}_i$ is the unit vector in the direction of spin magnetic moment at the site i. Furthermore, following previously adopted notations [24], we use vector symbols, such as $\vec{P}$, to denote polar vectors and bold symbols, such as $\boldsymbol{e}$, to denote pseudovectors.

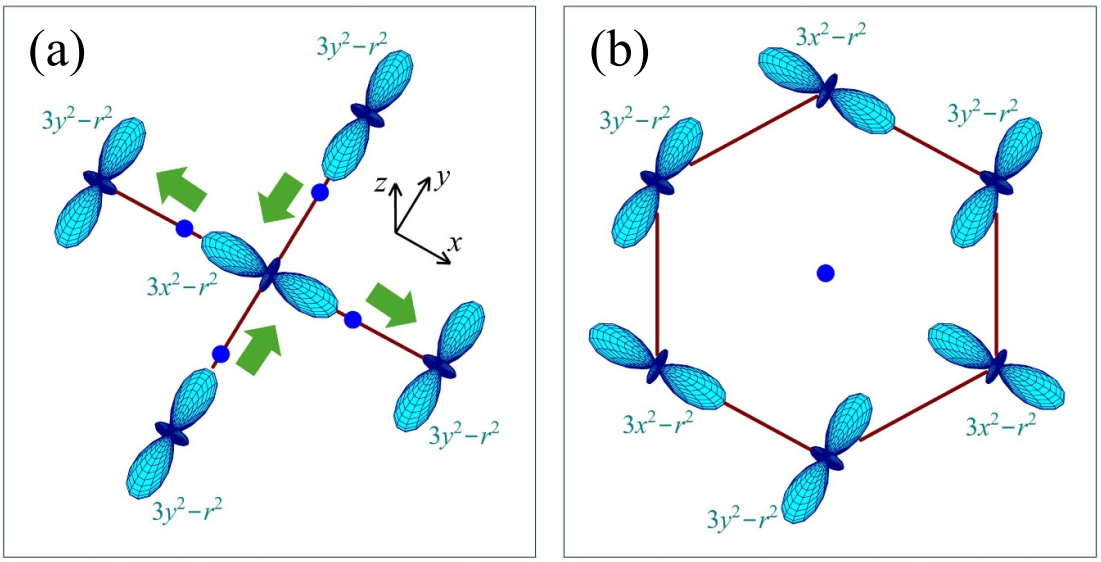

Figure 5. Example of the antiferro orbital order realized in perovskite (a) and honeycomb (b) lattice. In the perovskite lattice, the directions of polarization induced in each bond are shown by arrows. The inversion centers are shown by circles (which coincide with the positions of oxygen atoms in undistorted perovskite structure).

Then, using Slater–Koster parametrization in terms of $dd\sigma$ [37], one can find the following expressions for the transfer integral:

$$t_{ij}^{12} = \frac{1}{2}\sin\left(\vartheta_i - \vartheta_j\right) - \frac{1}{4}\sin\left(\vartheta_i + \vartheta_j\right) - \frac{\sqrt{3}}{4}\cos\left(\vartheta_i + \vartheta_j\right)$$

and the energy gain $\Delta E_{ij}^{\uparrow\uparrow} = -\frac{(t_{ij}^{12})^2 + (t_{ji}^{12})^2}{\tilde{U}}$ caused by the electron hoppings between occupied and unoccupied orbitals in the bond for the FM configuration of spins:

$$\Delta E_{ij}^{\uparrow\uparrow} = -\frac{4\sqrt{3}\sin 4\vartheta + \cos 4\vartheta - 2\cos 2\Delta\vartheta + 4}{\tilde{U}},$$

where $\vartheta = \frac{\vartheta_i + \vartheta_j}{2}$ and $\Delta\vartheta = \vartheta_i - \vartheta_j$. Minimizing $\Delta E_{ij}^{\uparrow\uparrow}$ with respect to ϑ and $\Delta\vartheta$, it is straightforward to find that $\vartheta = \frac{1}{4}\arctan(4\sqrt{3})$ and $\Delta\vartheta = \frac{\pi}{2}$, meaning that the orbital order is indeed of the antiferro type. Then, the electric polarization (the x component) in the bond can be found from equation (3) as

$$P_{ij}^{x} = -\frac{ea}{V\tilde{U}^2}\cos\left(2\vartheta + \frac{\pi}{3}\right),$$

where a is the bondlength.

5. Towards practical realization

In the previous section we have seen that the FM-FE state can be easily realized in the single bond by the antiferro orbital order. In this section, we will discuss whether such state can be realized in real materials having periodic structure.

5.1. Crystal lattice: perovskite versus honeycomb

The orbital order has been intensively studied in magnetoresistive manganites and other transition-metal compounds crystallizing in the perovskite structure [39–45]. Particularly, the antiferro orbital order is believed to be responsible for the FM character of exchange interactions in $LaMnO_3$ [13, 40], $YTiO_3$ [42], $LaVO_3$ [43], and YVO_3 [44]. However, in all these materials the magnetic atoms are located in the inversion centers. Therefore, although the electric polarization can be induced in each bond, there will always be another bond with the opposite direction of electric polarization, as explained in figure 5(a). Thus, most likely, these perovskite materials will be *antiferroelectric*. They can host very

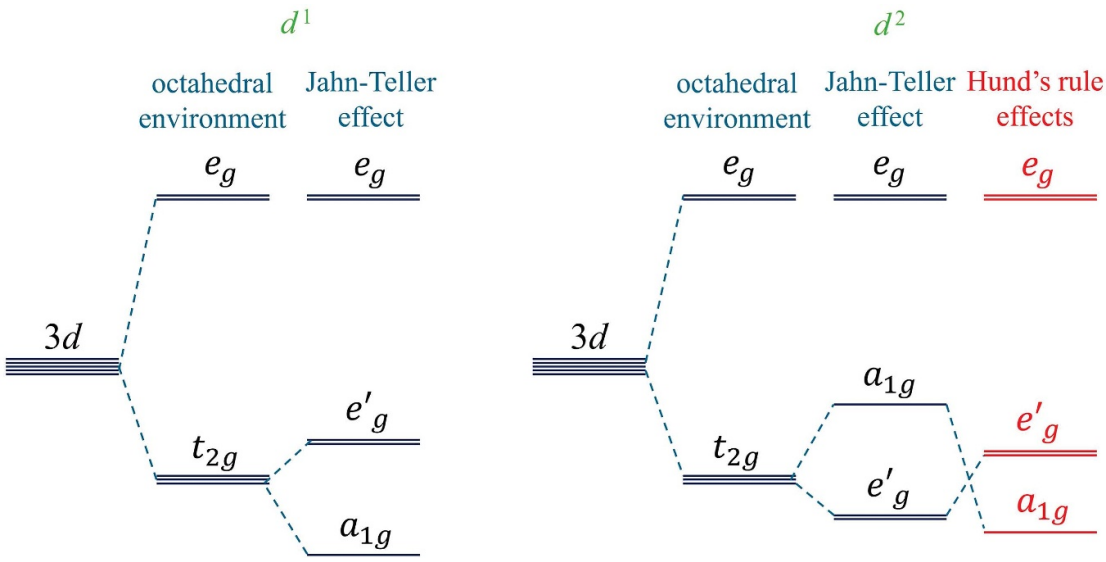

Figure 6. Atomic level splitting for electronic configurations d^1 (left) and d^2 (right). The octahedral environment of ligands around the transition-metal sites will split the $3d$ levels into threefold degenerate t_{2g} and twofold degenerate e_g states, correspondingly in the lower and upper part of the spectrum (the so-called $10Dq$ splitting). The Jahn–Teller distortion tends to lift the orbital degeneracy and further split the t_{2g} manifold into twofold degenerate e'_g and nondegenerate a_{1g} states ($\Delta_{\rm tr}$ splitting). This distortion works in the opposite directions for d^1 and d^2, stabilizing, respectively, a_{1g} and e'_g states. The d^2 configuration is subjected to atomic Hund's second rule effects, which tend to reenforce the ground state with maximal multiplicity and reverse the order of a_{1g} and e'_g states.

interesting properties, such as weak ferromagnetism, net orbital magnetization, etc [46], but hardly suitable from the viewpoint of FE applications.

The honeycomb lattice seems to be more promising. In this case, $\mathcal{I}$ connects two magnetic sublattices, while the atoms themselves are located not in the inversion centers, as explained in figure 5(b). Therefore, if we succeed in realizing the antiferro orbital order between the sublattices, our system can become simultaneously FM and FE.

5.2. Electronic configuration: d^1 versus d^2

The next important question is how to realize the antiferro orbital order on the honeycomb lattice. First, we explore the conventional picture based on the JT distortion, which takes place, for instance, in $LaMnO_3$ [47]. We assume that the transition-metal atoms are in the octahedral environment, which results in the $10Dq$ splitting of $3d$ levels into threefold degenerate t_{2g} and twofold degenerate e_g states, as explained in figure 6. Then, we consider the situation when there is either one or two $3d$ electrons residing in the t_{2g} shell, corresponding to the electronic configurations d^1 and d^2. Thus, the system is subjected to the JT distortion, which further splits degenerate t_{2g} levels into twofold degenerate e'_g and nondegenerate a_{1g} states. The corresponding parameter is denoted as $\Delta_{\rm tr}$. Moreover, the JT theorem states in this respect that the distorted system should have a nondegenerate ground state [48]. Therefore, the JT distortion should work in opposite directions for the configurations d^1 and d^2, stabilizing, respectively, a_{1g} and e'_g states (figure 6). Another important point is that for two sites connected by $\mathcal{I}$ the JT distortion is expected to be the same. Thus, the JT mechanism can stabilize ferro orbital order but not the antiferro one and alone does not break the inversion symmetry. Furthermore, since the ground state is nondegenerate, the orbital degrees of freedom are frozen. This suppress the Kugel–Khomskii mechanism of the orbital ordering when the latter is driven by superexchange processes.

Fortunately, the JT distortion is relatively weak in the t_{2g} systems so that other mechanisms can easily compete with it. One of such prominent mechanisms is Hund's second rule, driven by intraatomic interactions. In isolated atoms, the proper interaction parameter (the Racah parameter) is given by $B = \frac{9F^2-5F^4}{441}$, in terms of the radial Slater integrals F^2 and F^4 [49, 50]. For comparison, the intraatomic exchange coupling responsible for Hund's first rule is $J_{\rm H} = \frac{F^2+F^4}{14}$. Since $F^4 \sim 0.63F^2$ [36], the ratio $\frac{B}{J_{\rm H}}$ is about 0.1, which naturally explains the hierarchy of atomic Hund's rule, where the second rule should be considered only after the first one. Since for $3d$ ions $J_{\rm H} \sim 1$ eV [36, 39], B is about 0.1 eV. The important point is that typical crystal-field splitting of t_{2g} levels caused by the JT distortion is also of the order of 0.1 eV [45]. Therefore, these two mechanisms can compete with each other.

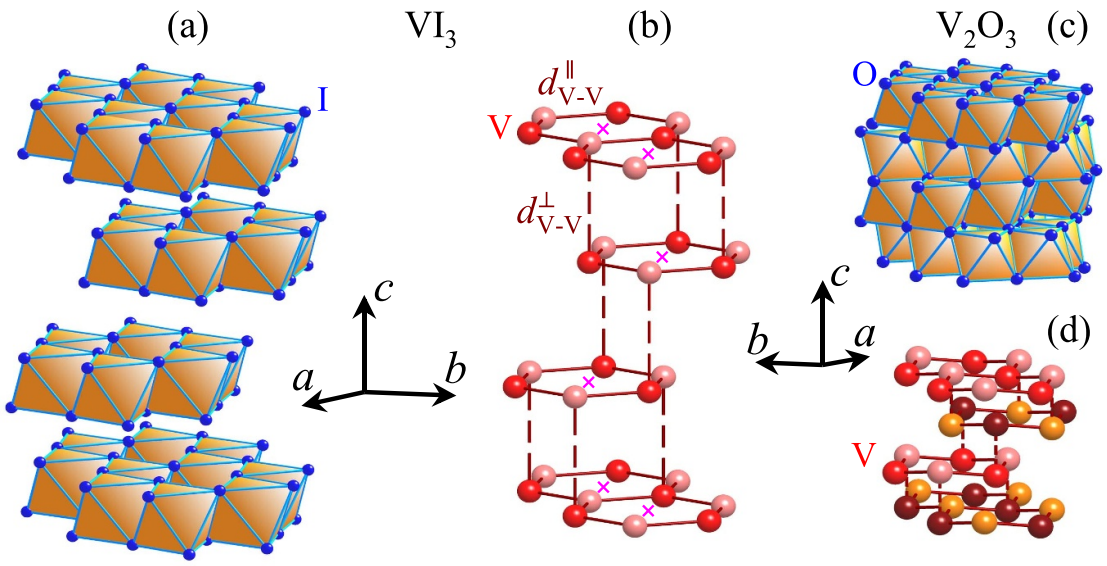

Figure 7. Crystal structure of VI_3 and V_2O_3. (a) Linked network of VI_6 octahedra in VI_3. (b) Vanadium atom positions in VI_3. Two sublattices are shown by different colors. $d^{\parallel}_{V-V}$ and $d^{\perp}_{V-V}$ are interatomic distances in and between the honeycomb planes. The inversion centers are denoted by ×. (c) Linked network of VO_6 octahedra in V_2O_3. (d) Vanadium atom positions in V_2O_3, where four sublattices are shown by different colors.

While the JT distortion tends to quench the orbital degrees in one particular configuration, Hund's second rule acts in the opposite direction and tends to realize the ground state with maximal orbital degeneracy. For the d^2 configuration, it can revert the order of the a_{1g} and e'_g levels. Therefore, in the atomic limit, one electron will reside on the nondegenerate a_{1g} orbital, while another one will be in the degenerate subspace spanned by two e'_g orbitals (see figure 6). A more rigorous picture can be obtained by considering exact two-electron states [11], following the arguments of Tanabe and Sugano [51]. This will reactivate the Kugel–Khomskii mechanism of the orbital ordering so that the occupied orbitals can adjust their shape to minimize the energy of exchange interactions and, hopefully, realize the antiferro order, breaking the inversion symmetry. Simple toy-model considerations supporting this idea can be found in [11].

The Hund's rules are essentially many-electron effects. They do not operate in the one-electron configuration d^1, where the JT distortion is the only mechanism that splits the t_{2g} levels. Therefore, in order to realize the antiferro orbital order on the honeycomb lattice, it is important to consider two-electron (or other) systems, in which Hund's rule effects are operative.

5.3. Details of electronic structure: VI_3 versus V_2O_3

In this section we will consider two potential d^2 candidates, VI_3 and V_2O_3, and argue that the antiferro orbital order stabilizing the FM-FE state can be probably realized in VI_3 but not in V_2O_3. The reason lies in details of the electronic structure, which is also related to the differences in the crystal structure and types of the ligand atoms.

VI_3 is the van der Waals material. At room temperature, it has $R\bar{3}$ structure [52], while V_2O_3 crystallizes in corundum $R\bar{3}c$ structure [53] (figure 7). The main structural motif of both VI_3 and V_2O_3 is the honeycomb planes formed by V^{3+} ions belonging to two different sublattices, which are connected by $\mathcal{I}$. The ions in the same sublattices are connected by threefold rotations and translations. In V_2O_3, the situation is additionally complicated by the fact that there are two pairs of the V^{3+} sublattices forming alternating honeycomb planes as shown in figure 7(d). In any case, as long as we consider only the V^{3+} ions, the stacking of honeycomb planes looks very similar in VI_3 and V_2O_3. The main difference lies in the packing of the VI_6 and VO_6 octahedra in the van der Waals and corundum structure. In the former case, the octahedra form edge-sharing network in the honeycomb planes, but remains disconnected in the c direction. However, in the corundum structure of V_2O_3, some of the VO_6 octahedra belonging to adjacent honeycomb planes share their faces [54]. It has strong impact on the V–V distances in ($d^{\parallel}_{V-V}$) and between ($d^{\perp}_{V-V}$) the planes. In the van der Waals structure of VI_3, $d^{\perp}_{V-V} = 6.55$ Å is substantially larger than $d^{\parallel}_{V-V} = 3.95$ Å, whereas in V_2O_3, $d^{\perp}_{V-V} = 2.71$ Å is even shorter than $d^{\parallel}_{V-V} = 2.88$ Å. Thus, in

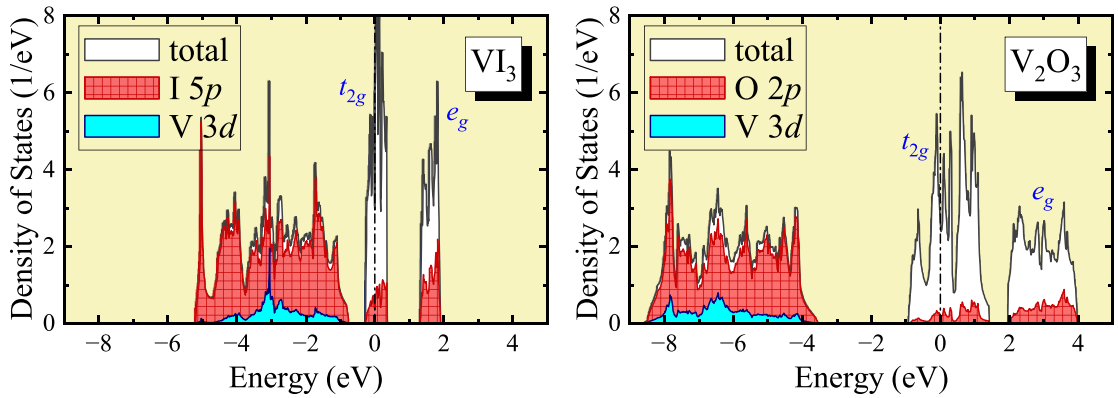

Figure 8. Total and partial densities of states of VI_3 and V_2O_3 in the local density approximation. The Fermi level is at zero energy (shown by dot-dashed line). The $10Dq$ splitting leads to the formation of two distinct V $3d$ bands denoted as t_{2g} and e_g.

Table 1. Parameters of model Hamiltonian for V_2O_3 and VI_3 (in eV): trigonal splitting between e_g' and a_{1g} states ($\Delta_{\rm tr}$), $10Dq$ splitting between t_{2g} and e_g states, on-site Coulomb repulsion U, intraatomic exchange coupling $J_{\rm H}$ responsible for Hund's first rule, and Racah parameter B responsible for Hund's second rule. Reproduced from [11]. CC BY 4.0.

compound	$\Delta_{\rm tr}$	$10Dq$	U	$J_{\rm H}$	B
V_2O_3	0.15	2.31	3.05	0.85	0.09
VI_3	0.01	1.49	1.21	0.75	0.07

V_2O_3, $d^{\perp}_{\rm V-V}$ is the additional parameter of the crystal structure, which strongly influences the orbital order and can even result in the formation of molecular states shared by two V^{3+} [55, 56]. Since the I $5p$ states are rather diffuse, the d–p hybridization is weaker in VI_3, which is also reflected in longer V–V distances.

Furthermore, the electronic structure appears to be rather different in VI_3 and V_2O_3 (see figure 8).

Using the electronic structure in the local density approximation (LDA), one can construct the effective model for the V $3d$ bands in VI_3 and V_2O_3, which are primarily responsible for the magnetism. Namely, the one-electron parameters can be related to the matrix elements of LDA Hamiltonian in the Wannier basis for the V $3d$ bands located in the interval $[-0.5, 2]$ eV for VI_3 and $[-1, 4]$ eV for V_2O_3. The effective Coulomb interactions can be evaluated using constrained random-phase approximation (cRPA) [57]. Technical details can be found in [45] and [11].

The model parameters depend on the electronic structure, which explains the sharp difference between VI_3 and V_2O_3 (see figure 8 and table 1). Namely:

- The interaction parameters for V $3d$ bands in cRPA depend on how well they are screened by other bands, particularly by O $2p$ and I $5p$ bands. The closer the bands are, the stronger the screening. Thus, the parameters U, $J_{\rm H}$, and B are generally weaker in VI_3 (table 1). Moreover, $J_{\rm H}$ and B are typically less screened than U. Therefore, the ratio $\frac{J_{\rm H}}{U}$ is substantially larger in VI_3, which is important for stabilizing FM interactions [19];
- The trigonal splitting between e_g' and a_{1g} states ($\Delta_{\rm tr}$) is substantially smaller in VI_3, so that $\frac{\Delta_{\rm tr}}{B} < 1$ in VI_3 but > 1 in V_2O_3 (table 1). This will reactivate the Kugel–Khomskii mechanism and drive the formation of antiferro orbital order in VI_3 but not in V_2O_3;
- $10Dq$ splitting is also smaller in VI_3. This facilitates the mixing of the e_g' and e_g states belonging to the same representation by Hund's rule interactions and further minimizes the energy of these interactions. This further support the Kugel–Khomskii mechanism and formation of antiferro orbital order in VI_3.

Thus, VI_3 appears to be a good candidate for spontaneous breaking of inversion symmetry by the antiferro orbital order and realizing the FM-FE state. The d^2 configuration itself does not necessarily guarantee the emergence of antiferro orbital order, where many things depend on details of the electronic structure.

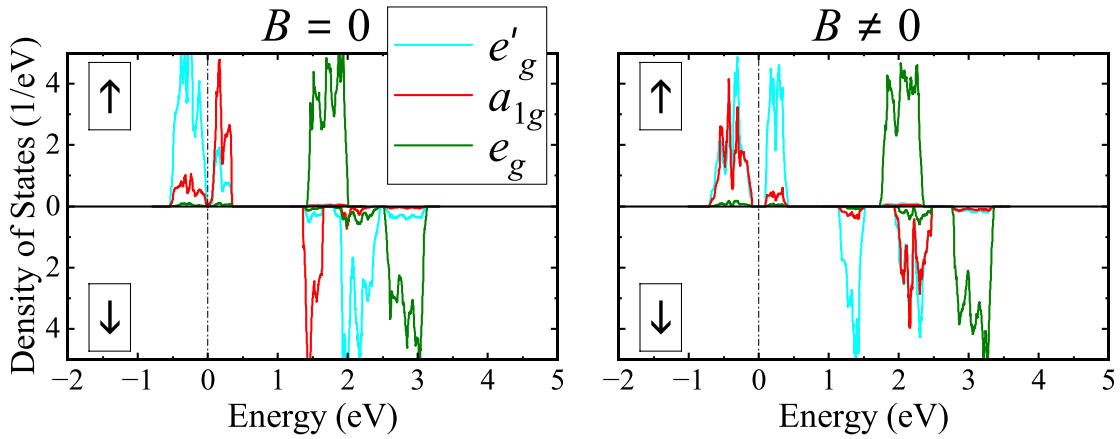

Figure 9. Total and partial densities of states as obtained in the Hartree–Fock approximation for the ferromagnetic state, where the Racah parameter B responsible for Hund's second rule was set to either 0 (left) or 0.07 eV (right). The Fermi level is at zero energy (the middle of the band gap). Reproduced from [11]. CC BY 4.0.

The lattice distortion seems to be also different in VI_3 and V_2O_3. Below 150 K, the corundum structure of V_2O_3 undergoes a monoclinic distortion [58], which further stabilize the e_g' levels, following the JT theorem [48]. The experimentally observed AFM order can be successfully explained by details of this monoclinic structure [56]. On the other hand, the lattice distortion in VI_3 is a matter of controversy, which will be briefly discussed in section 7. It can be the sign of orbital degeneracy, which can lead to the realization of the FE-FM state as we propose [11].

6. What can one expect from VI_3?

Finally, we turn to numerical mean-field Hartree–Fock (HF) calculations for the model, which was obtained for the V $3d$ bands of VI_3 as described above [11]. Some of the model parameters are summarized in table 1. The total energy in the HF approximation is expressed in terms of the one-electron density matrix at each site of the lattice, $\hat{n} = [n_{ab}^{\sigma\sigma'}]$, which is calculated self-consistently, where a and b are the orbital indices (two e_g, one a_{1g}, and two e_g'), while σ and σ' are the spin indices ($\uparrow$ or $\downarrow$). The nondiagonal matrix elements with respect to $\uparrow$ and $\downarrow$ are typically induced by relativistic spin-orbit (SO) interaction. Otherwise, $\hat{n}$ is diagonal. The details can be found in [45].

The corresponding densities of states for the FM state with and without the on-site interactions responsible for Hund's second rule are shown in figure 9. The strength of these interactions is controlled by the Racah parameter B. As expected, when $B = 0$, the type of occupied states is solely determined by weak trigonal splitting $\Delta_{\rm tr}$, so that two $3d$ electrons tend to occupied twofold degenerate e_g' states. Therefore, the ground state appears to be nondegenerate. The a_{1g} states are located mainly in the unoccupied part and mixed with e_g' ones by intersite hoppings. However, the situation changes dramatically when B is finite, as schematically explained in figure 6. In this case, two $3d$ electrons reside on the a_{1g} orbital and one of the e_g' orbital. Thus, the ground state is degenerate. The shape of the occupied e_g' states is controlled by superexchange interactions, which further lower the energy via the antiferro orbital ordering [17–19].

Similar picture can be obtained using more sophisticated dynamical mean-field theory [11].

6.1. Orbital ordering and inversion symmetry breaking

Let us start with restricted HF calculations without SO interaction, where we additionally constrain the form of $\hat{n}$ to satisfy the $R\bar{3}$ symmetry of VI_3 lattice. Technically, $\hat{n}$ is averaged by the matrices of threefold rotations in each sublattices to guarantee the $R3$ symmetry. Then, $\hat{n}$ is averaged over the sublattices to guarantee the inversional symmetry. This $R\bar{3}$ solution is regarded as the reference point (figure 10).

Then, we relax the constraints. First, we turn off the rotational constraint and average $\hat{n}$ only over the sublattices, enforcing the inversional invariance. The atoms within the sublattices are connected by translations, but no longer by the threefold rotations. The corresponding symmetry

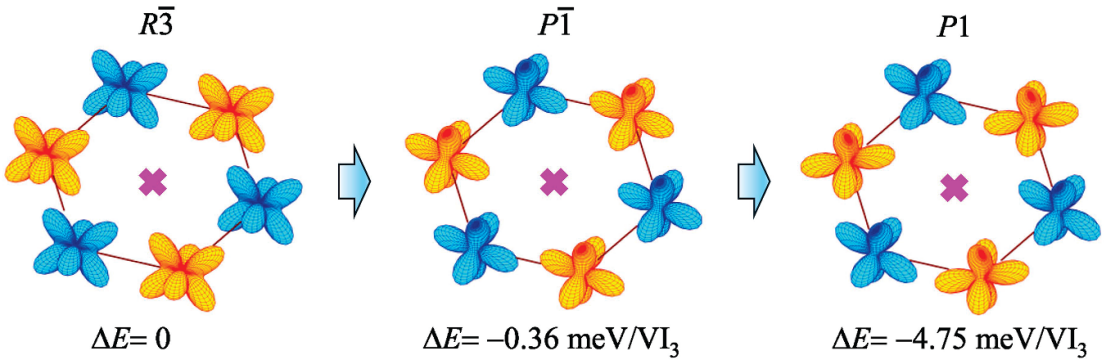

Figure 10. Orbital ordering in the ferromagnetic state of VI_3 as obtained in model Hartree–Fock calculations by enforcing the original trigonal $R\bar{3}$ symmetry, the triclinic $P\bar{1}$ symmetry, and fully relaxing the symmetry ($P1$). The crystallographic inversion centers are denoted by $\times$. To sublattices of honeycomb lattice are displayed by different colors. ΔE is the corresponding energy change relative to the state with the $R\bar{3}$ symmetry. Reproduced from [11]. CC BY 4.0.

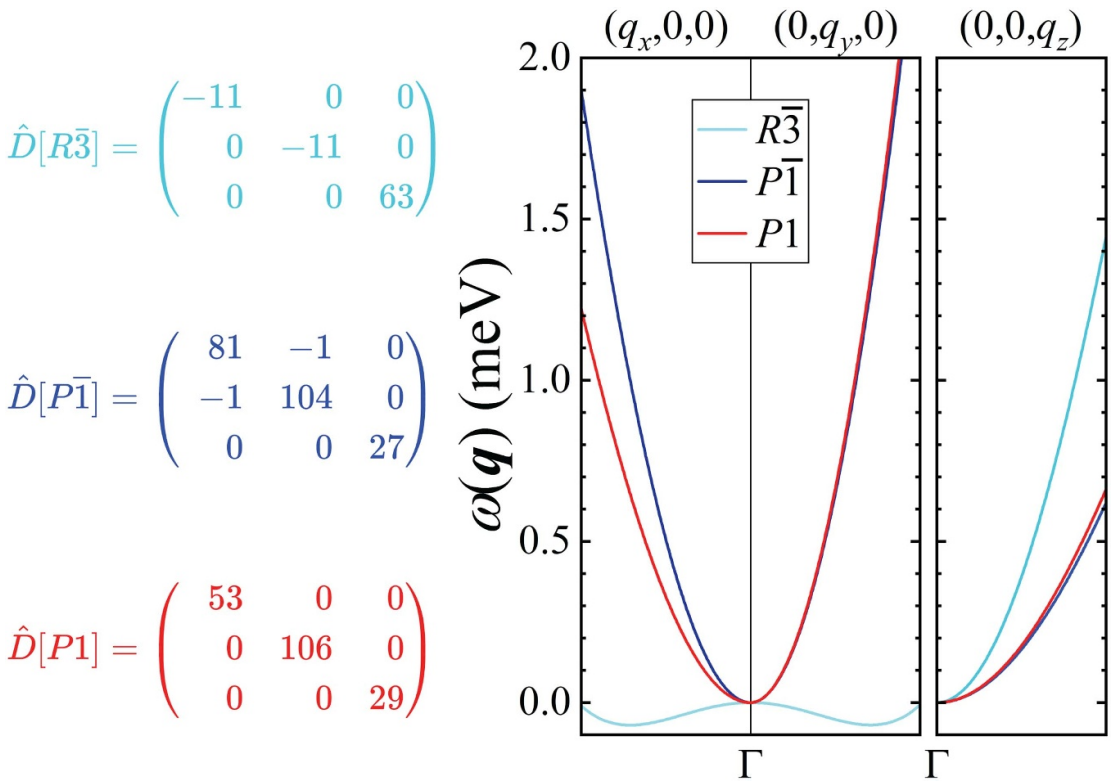

Figure 11. Spin-wave stiffness tensors (in meVÅ^2) for the orbital states of the $R\bar{3}$, $P\bar{1}$, and $P1$ symmetry, and corresponding spin-wave dispersions near the Γ-point of Brillouin zone. Reproduced from [11]. CC BY 4.0.

of the orbital order is $P\bar{1}$. It changes the shape of the occupied orbitals, but only slightly lowers the energy.

Finally, we relax the inversional constraint and treat $\hat{n}$ in two sublattices as independent variables. The corresponding symmetry is $P1$. In comparison with the $P\bar{1}$ state, the occupied orbitals in two sublattices are additionally rotated relative to each other, so that $\mathcal{I}$ becomes broken, resulting in significant energy gain (figure 10).

The next important question is whether the FM spin order is stable or not. The answer depends on the spin-wave stiffness $\hat{D}$, which can be evaluated using linear response theory for interatomic exchange interaction [59]. In the present context, it is basically a perturbation theory with respect to infinitesimal rotations of spins. If $\hat{D}$ is positive definite, the FM order is stable. If not, it is unstable. The results are summarized in figure 11. One can clearly see that the FM state is unstable if the orbital configuration respects the $R\bar{3}$ symmetry of the lattice. Nevertheless, lowering the orbital symmetry will stabilize the FM state.

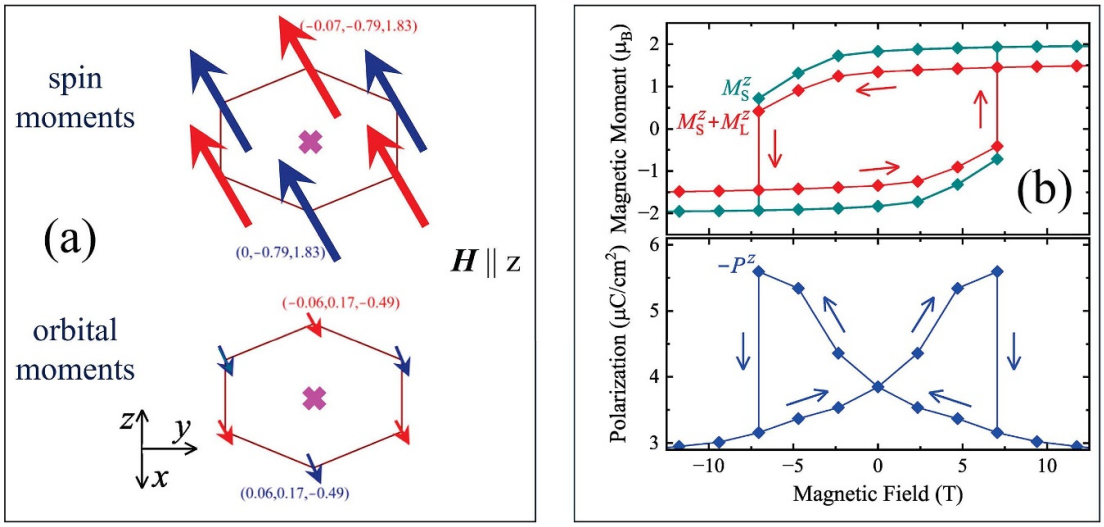

Figure 12. Results of Hartree–Fock simulations with spin–orbit interaction and magnetic field. (a) Directions of spin ($\boldsymbol{M}_S$) and orbital ($\boldsymbol{M}_L$) magnetic moments without magnetic field. Two sublattices are denoted by red and blue colors. The numerical values of $\boldsymbol{M}_S$ and $\boldsymbol{M}_L$ are given in parentheses. The crystallographic inversion center is denoted by ×. (b) Magnetic-field dependence of magnetization (top) and electric polarization (bottom). The field is applied parallel to z. M_S^z, $M_S^z + M_L^z$, and P^z are the values of, respectively, spin magnetic moment, total magnetic moment, and electric polarization along z. Reproduced from [11].

6.2. Magnetic field control of electric polarization

In the previous section we have seen that, in the FM state of VI_3, $\mathcal{I}$ can be broken by the orbital order. The next important questions are: (i) how large is the electric polarization? (ii) How can it be controlled by a magnetic field?

The key point here is that the orbital order breaks not only inversional but also the threefold rotational symmetry. Therefore, the magnetic moments are not necessarily aligned perpendicular to the honeycomb plane or lie in this plane (figure 12). Since the rotational symmetry is broken by the orbital order, the a_{1g} and e_g' states do not longer belong to different representations and are allowed to mix. The angle between magnetic moments and the hexagonal z-axis is induced by the SO interaction and depends on the degree of this mixing. This angle can be also controlled by the external magnetic field $\boldsymbol{H} = (0, 0, H)$ along z. Therefore, $\boldsymbol{H}$ can be also used to control the electronic degrees of freedom, such as the a_{1g}–e_g' mixing and the polarization $\vec{P}$. This is the main mechanism of magneto-electric coupling in the symmetry-broken state of VI_3. Furthermore, besides spin magnetic moment, $|\boldsymbol{M}_S| \sim 2\ \mu_B$, there is an appreciable orbital magnetic moment, $|\boldsymbol{M}_L| \sim 0.5\ \mu_B$, induced by the SO coupling and further enhanced by electron–electron interactions on V sites [60, 61]. The inversion symmetry breaking gives rise to an effective Dzyaloshinskii–Moriya interaction, which is responsible for small canting of magnetic moments between different sublattices (figure 12). Contrary to regular Dzyaloshinskii–Moriya interactions [62, 63], caused by off-centrosymmetric displacements of intermediate ligand sites [64], these interactions are induced solely by antiferro orbital ordering.

Results of numerical simulations in the magnetic field are summarized in figure 12. The electric polarization was evaluated using Berry-phase theory, which was applied to the model Hamiltonian in the HF approximation [65]. Since threefold rotational symmetry is broken, $\vec{P}$ is allowed to have all three components. Here, we focus on the behavior of P^z, which dominates over P^x and P^y [11]. The magnetic field dependence of spin and orbital magnetic moments is characterized by the hysteresis loop, where the field applied in the positive direction of z leads to the saturation of magnetization, while in the opposite direction it leads to the reorientation of magnetization at around $H \sim -7$ T. Corresponding P^z has a characteristic butterflylike shape and undergoes the jump $\Delta P^z \sim 2.4\,\mu\mathrm{C\,cm^{-2}}$ at the point of reorientation of the magnetization. This polarization jump is comparable with the one observed in $CaBaCo_4O_7$ ($\Delta P \sim 1.7\,\mu\mathrm{C\,cm^{-2}}$), which is believed to be the largest polarization change induced by magnetic field [66].

7. Summary and outlook

First, let us summarize main principles for realizing orbitally induced FM-FE state, which we propose.

(i) The magnetic atoms should not be in the inversion centers. Different atoms in the lattice can be connected by $\mathcal{I}$, and this $\mathcal{I}$ can be broken by antiferro orbital order. One promising example of such lattice is the honeycomb plane, considered in the present work. Of course, there are other possibilities including corundum, some hexagonal and monoclinic lattices realized, for instance, in the $P6_3/mmc$ phase of $BaCrO_3$ [67] and $P2/c$ phase of $CoWO_4$ [68].

(ii) The d^2 configuration appears to be rather unique, at least for the octahedral environment. Two electrons are required to activate Hund's second rule and enforce the orbital degeneracy, so that the occupied orbitals could freely adjust their shape and minimize the energy of exchange interactions via the orbital ordering. From this point of view, other configurations are less promising. The d^1 configuration can be excluded because single electron is not subjected to the Hund's rule physics. The level splitting in this case is controlled solely by the JT distortion, which lifts the orbital degeneracy, preventing the system from formation of the antiferro orbital order. A similar situation occurs for the d^4 configuration in the high spin-state, where there is only one hole in the majority-spin shell and, therefore, no room for realizing Hund's second rule. Furthermore, the d^4 configuration is subjected to strong JT distortion [47]. The d^3 configuration is not orbitally active because of large $10Dq$ splitting. Thus, considering less than half filled shell in octahedral environment, the only promising configuration seems to be d^2, which can be realized in Ti^{2+}, V^{3+}, and Cr^{4+}.

(iii) The main parameters controlling the ground state of the d^2 ions are Δ_{tr}, B, and $10Dq$. The crystal-field splitting Δ_{tr} is caused by the JT distortion, which tends to lift the orbital degeneracy. The Racah parameter B is responsible for Hund's second rule, which acts in the opposite direction, yielding the ground state with maximal orbital degeneracy. The octahedral splitting $10Dq$ does not alter the order of t_{2g} levels directly. However, since Hund's interactions mix the e_g' and e_g states, which are separated by $10Dq$, the strength of the Hund's rule coupling effectively depends on $10Dq$. Hund's second rule does not apply to isolated t_{2g} manifold in the limit of large $10Dq$: the situation is similar to p electron system, where for the high-spin state there is always only one possible orbital state. Therefore, mixing of the e_g' and e_g states is crucial for realizing Hund's second rule. While B is not sensitive to the crystal environment, Δ_{tr} and $10Dq$ strongly depend on details of the crystal structure and type of the ligand atoms. For our purposes, one would like to have smaller Δ_{tr} and $10Dq$. Since they depend on the hybridization between transition-metal d and ligand p states, the I^- ions seem to be more promising than O^{2-}: the I $5p$ states are more diffuse, the V–I distance is significantly larger and, therefore, the hybridization between V $3d$ and I $5p$ states is substantially weaker.

(iv) Another interesting option is the d^7 configuration of Co^{2+} ions in the honeycomb lattice. Such materials are well know and widely discussed as potential candidates for realizing the Kitaev quantum spin liquid state [69, 70]. The canonical examples are $BaCo_2(AsO_4)_2$ [71] and $Na_2Co_2TeO_6$ [72]. The corresponding Kitaev model is formulated for the Co^{2+} ions having pseudospin-1/2 doublet in the ground state, which can be realized in the large $10Dq$ limit. However, in order to realize the antiferro orbital order on the honeycomb lattice via Hund's second rule, we need the opposite situation with relatively small $10Dq$, which will mix the pseudospin-1/2 doublet with other states. Thus, materials suitable for the FM-FE state are generally unsuitable for the Kitaev physics (and vice versa).

To date, VI_3 remains the only potential candidate for realizing the orbitally induced FM-FE state [11]. Nevertheless, the experimental situation is rather controversial. VI_3 is indeed a ferromagnet with relatively high Curie temperature, $T_C \approx 50$ K [73]. Besides the FM transition, VI_3 exhibits at least two structural phase transitions, at around 78 and 32 K [74, 75]. Details of these transitions is a matter of dispute: there exist different proposals regarding crystal structure changes, the direction of these changes, as well as their interconnection with the magnetic properties of VI_3 [11]. There are several suggestions that the vanadium atoms across inversion centers in honeycomb layers become inequivalent, either structurally [76] or magnetically [77], meaning that these inversion centers are broken and the material can be potentially FE. In any case, the experimental data seems to suggest that the crystal structure of VI_3 is rather fragile, which is consistent with our main idea that the orbital degrees of freedom in VI_3 remain active and the decision which orbitals become occupied and which remain empty may depend on tiny balance between several factors, including the experimental conditions.

It remains an open question whether the above principles (i)–(iv) are sufficient for realizing the FM-FE ground state in VI_3 and related materials. The orbital degeneracy is the very challenging theoretical problem and there are various scenarios of how this degeneracy is resolved and what will be the consequences for the properties of real materials [78]. Nevertheless, we believe that the FM ferroelectricity is one the plausible scenarios, that should be carefully considered alongside with others.

Besides FM ferroelectricity, there are other interesting fundamental issues related to the Hund's rule physics. The importance of Hund's first rule in the physics of strongly correlated materials is well recognized today [79]. These effects are driven by interatomic exchange coupling $J_{\rm H}$. However, the consequences of Hund's second rule, driven by the Racah parameter B, remain largely unexplored. Due to the hierarchy of atomic Hund's rules, reflected in the condition $B \sim 0.1J_{\rm H}$, the Hund's second rule effects should emerge on much smaller energy scale, which posses a challenge for numerical simulations. Nevertheless, the implication of these effects to the physics of strongly correlated materials is rather interesting, as they provide a possibility for realizing new phenomena, such as FE ferroelectricity. They also provide a new look on other canonical problems.

Particularly, orbital fluctuations were and continue to be the hot topic in the physics of t_{2g} perovskite oxides, like $LaVO_3$ and YVO_3 [78]. One of the key questions is how well these fluctuations are quenched by the lattice distortions, which are typically present in these systems. The analysis of the crystal-field splitting, derived from the electronic structure calculations, suggests that it can be quite strong [45]. However, this analysis was typically based on the minimal three-orbital model constructed for the t_{2g} bands, which excludes the effects of Hund's second rule. On the other hand, Hund's second rule is expected to play an important role in these two-electron materials and compete with the crystal field. Thus, the problem of orbital fluctuations in $LaVO_3$ and YVO_3 can be reconsidered on a new level, taking into consideration the Hund's second rule effects in a more general model constructed simultaneously for the t_{2g} and e_g bands. One of the key parameters of such model controlling the strength of effective interactions responsible for Hund's second rule will be $10Dq$.

Another seminal problem is how to improve the exchange-correlation functional in first-principles electronic structure calculations in order to deal with the orbital magnetism. The density functional theory, providing general foundation for modern electronic structure calculations, is formally exact. However, to be practically applicable, it is supplemented with additional approximations, such as local spin density approximation (LSDA) or generalized gradient approximation (GGA), which largely rely on the model of electron gas and fail to account properly for the physics of intraatomic interactions, including those responsible for Hund's second rule. Very often, the orbital magnetization calculated within LSDA or GGA is severely underestimated. In order to circumvent this problem, one popular strategy was to mimic the effects of Hund's second rule in electronic structure calculations, by adding a phenomenological term, which would (i) be proportional to the Racah parameter B and (ii) tend to enhance $\boldsymbol{M}_{\rm L}$ [80–82]. The typical choice is $-B\boldsymbol{M}_{\rm L}^2$ [80, 81], similar to the Stoner theory of spin magnetism, though there were also other suggestions [82]. Another contribution to the orbital magnetization is driven by the on-site Coulomb repulsion U [60, 61, 83]. It does not contribute to the energy of isolated atoms with the given integer number of electrons [36], but emerges in solids, where the atoms can freely exchange electrons. The key question in this context is how to properly evaluate the screening of U, especially in metallic systems [84].

By treating U as an adjustable parameter, as is frequently done in electronic structure calculations, one can easily reproduce the experimental magnetization. However, it does not bring us closer to microscopic understanding of this problem because there can be other interactions controlling the value of $\boldsymbol{M}_{\rm L}$. Particularly, what is the relative importance of on-site Coulomb repulsion U and interactions responsible for Hund's second rule? In this respect, one should clearly understand that the proposed correction $-B\boldsymbol{M}_{\rm L}^2$ is totally empirical and does not deal with the true physics of atomic Hund's rules. For instance, it will enhance $\boldsymbol{M}_{\rm L}$ even when there is only one electron, which does not obey any Hund's rules. However, it does not mean that Hund's rule interactions cannot contribute to $\boldsymbol{M}_{\rm L}$ in principle. A much better solution of the problem can be obtained by considering intraatomic exchange interaction energy in the HF approximation, which treats on an equal footing all three parameters: U, $J_{\rm H}$, and B [60, 61]. The applications can be also rather interesting. For instance, one can expect that the orbital magnetization in the d^1 and d^2 materials should behave differently: in the former case, it is controlled solely by Coulomb U, while in the latter case there will be an additional contribution associated with Hund's second rule.

Acknowledgments

I am indebted to Ryota Ono and Sergey Nikolaev for collaboration on earlier stages of this project [11]. MANA is supported by World Premier International Research Center Initiative (WPI), MEXT, Japan.

Data availability statement

The data cannot be made publicly available upon publication because they are not available in a format that is sufficiently accessible or reusable by other researchers. The data that support the findings of this study are available upon reasonable request from the authors.

Author contribution

I V Solovyev 0000-0002-2010-9877
Conceptualization (lead), Formal analysis (lead), Investigation (lead), Methodology (lead), Validation (lead), Visualization (lead), Writing – original draft (lead), Writing – review & editing (lead)

References

[1] Tokura Y 2006 *Science* **312** 1481
[2] Cheong S-W and Mostovoy M 2007 *Nat. Mater.* **6** 13
[3] Khomskii D 2009 *Physics* **2** 20
[4] Tokura Y, Seki S and Nagaosa N 2014 *Rep. Prog. Phys.* **77** 076501
[5] Hill N 2000 *J. Phys. Chem. B* **104** 6694
[6] Seshadri R and Hill N A 2001 *Chem. Mater.* **13** 2892
[7] Fennie C J and Rabe K M 2006 *Phys. Rev. Lett.* **97** 267602
[8] Lee J H and Rabe K M 2010 *Phys. Rev. Lett.* **104** 207204
[9] Edström A and Ederer C 2018 *Phys. Rev. Matter.* **2** 104409
[10] Vaz C A F and Staub U 2013 *J. Mater. Chem. C* **1** 6731
[11] Solovyev I V, Ono R and Nikolaev S A 2024 *Phys. Rev. B* **110** 205116
[12] Anderson P W 1950 *Phys. Rev.* **79** 350
[13] Goodenough J B 1955 *Phys. Rev.* **100** 564
[14] Goodenough J B 1958 *J. Phys. Chem. Solids* **6** 287
[15] Kanamori J 1959 *J. Phys. Chem. Solids* **10** 87
[16] Day C 2024 *Physics* **17** s131
[17] Kugel K I and Khomskii D I 1972 *JETP Lett.* **15** 446 (available at: http://jetpletters.ru/ps/1754/article_26676.shtml)
[18] Khomskii D I and Kugel K I 1973 *Solid State Commun* **13** 763
[19] Kugel K I and Khomskii D I 1982 *Sov. Phys. Usp.* **25** 231
[20] King-Smith R D and Vanderbilt D 1993 *Phys. Rev. B* **47** 1651(R)
[21] Resta R 1994 *Rev. Mod. Phys.* **66** 899
[22] Ono R, Nikolaev S and Solovyev I 2020 *Phys. Rev. B* **102** 064422
[23] Solovyev I, Ono R and Nikolaev S 2021 *Phys. Rev. Lett.* **127** 187601
[24] Solovyev I V 2025 *Condens. Matter* **10** 21
[25] Lines M E and Glass A M 2004 *Principles and Applications of Ferroelectrics and Related Materials* (Clarendon)
[26] Bersuker I B 1966 *Phys. Lett.* **20** 589
[27] Cohen R E 1992 *Nature* **358** 136
[28] Öpik U and Pryce M H L 1957 *Proc. R. Soc. A* **238** 425
[29] Bersuker I B 2012 *Phys. Rev. Lett.* **108** 137202
[30] Kimura T, Goto T, Shintani H, Ishizaka K, Arima T and Tokura Y 2003 *Nature* **426** 55
[31] Tokura Y and Seki S 2010 *Adv. Mater.* **22** 1554
[32] Katsura H, Nagaosa N and Balatsky A V 2005 *Phys. Rev. Lett.* **95** 057205
[33] Xiang H J, Kan E J, Zhang Y, Whangbo M-H and Gong X G 2011 *Phys. Rev. Lett.* **107** 157202
[34] Kaplan T A and Mahanti S D 2011 *Phys. Rev. B* **83** 174432
[35] Anderson P W 1959 *Phys. Rev.* **115** 2
[36] Solovyev I V, Dederichs P H and Anisimov V I 1994 *Phys. Rev. B* **50** 16861
[37] Slater J C and Koster G F 1954 *Phys. Rev.* **94** 1498
[38] Solovyev I V and Terakura K 1998 *J. Korean Phys. Soc.* **33** 375 (available at: https://www.jkps.or.kr/journal/view.html?uid=3126&vmd=Full)
[39] Khomskii D I and Streltsov S V 2021 *Chem. Rev.* **121** 2992
[40] Solovyev I, Hamada N and Terakura K 1996 *Phys. Rev. Lett.* **76** 4825
[41] Maezono R, Ishihara S and Nagaosa N 1998 *Phys. Rev. B* **58** 11583
[42] Mochizuki M and Imada M 2003 *Phys. Rev. Lett.* **91** 167203
[43] Sawada H, Hamada N, Terakura K and Asada T 1996 *Phys. Rev. B* **53** 12742
[44] Blake G R, Palstra T T M, Ren Y, Nugroho A A and Menovsky A A 2001 *Phys. Rev. Lett.* **87** 245501
[45] Solovyev I V 2008 *J. Phys.: Condens. Matter* **20** 293201
[46] Solovyev I V 2025 arXiv:2509.00369
[47] Kanamori J 1960 *J. Appl. Phys.* **31** S14
[48] Jahn H A and Teller E 1937 *Proc. R. Soc. A* **161** 220
[49] Racah G 1942 *Phys. Rev.* **62** 438
[50] Slater J C 1960 *Quantum Theory of Atomic Structure* (McGraw-Hill)
[51] Tanabe Y and Sugano S 1954 *J. Phys. Soc. Japan* **9** 766
[52] Tian S, Zhang J-F, Li C, Ying T, Li S, Zhang X, Liu K and Lei H 2019 *J. Am. Chem. Soc.* **141** 5326
[53] Roziera P, Ratusznab A and Galy J 2002 *Z. Anorg. Allg. Chem.* **628** 1236

[54] Mattheiss L F 1994 *J. Phys.: Condens. Matter* **6** 6477
[55] Castellani C, Natoli C R and Ranninger J 1978 *Phys. Rev. B* **18** 4945
[56] Ezhov S Y, Anisimov V I, Khomskii D I and Sawatzky G A 1999 *Phys. Rev. Lett.* **83** 4136
[57] Aryasetiawan F, Imada M, Georges A, Kotliar G, Biermann S and Lichtenstein A I 2004 *Phys. Rev. B* **70** 195104
[58] Dernier P D and Marezio M 1970 *Phys. Rev. B* **2** 3771
[59] Solovyev I V 2024 *J. Phys.: Condens. Matter* **36** 223001
[60] Solovyev I V, Liechtenstein A I and Terakura K 1998 *Phys. Rev. Lett.* **80** 5758
[61] Solovyev I V 2014 *Phys. Rev. B* **90** 024417
[62] Dzyaloshinsky I 1958 *J. Chem. Phys. Solids* **4** 241
[63] Moriya T 1960 *Phys. Rev.* **120** 91
[64] Keffer F 1962 *Phys. Rev.* **126** 896
[65] Solovyev I V, Valentyuk M V and Mazurenko V V 2012 *Phys. Rev. B* **86** 144406
[66] Caignaert V, Maignan A, Singh K, Simon C, Pralong V, Raveau B, Mitchell J F, Zheng H, Huq A and Chapon L C 2013 *Phys. Rev. B* **88** 174403
[67] Chamberland B L 1982 *J. Solid State Chem.* **43** 309
[68] Xiao E-C, Liu M, Ren Q, Cao Z, Guo M, Dou G, Qi Z-M and Shi F 2020 *Ceram. Int.* **46** 15705
[69] Liu H and Khaliullin G 2018 *Phys. Rev. B* **97** 014407
[70] Sano R, Kato Y and Motome Y 2018 *Phys. Rev. B* **97** 014408
[71] Zhong R, Gao T, Ong N P and Cava R J 2020 *Sci. Adv.* **6** eaay6953
[72] Lin G *et al* 2021 *Nat. Commun.* **12** 5559
[73] Kong T, Stolze K, Timmons E I, Tao J, Ni D, Guo S, Yang Z, Prozorov R and Cava R J 2019 *Adv. Mater.* **31** 1808074
[74] Dolezal P *et al* 2019 *Phys. Rev. Matter.* **3** 121401(R)
[75] Marchandier T, Dubouis N, Fauth F, Avdeev M, Grimaud A, Tarascon J-M and Rousse G 2021 *Phys. Rev. B* **104** 014105
[76] Son S *et al* 2019 *Phys. Rev. B* **99** 041402(R
[77] Gati E, Inagaki Y, Kong T, Cava R J, Furukawa Y, Canfield P C and Bud'ko S L 2019 *Phys. Rev. B* **100** 094408
[78] Khaliullin G 2005 *Prog. Theor. Phys. Supp.* **160** 155
[79] Georges A, de' Medici L and Mravlje J 2013 *Annu. Rev. Condens. Matter Phys.* **4** 137
[80] Eriksson O, Johansson B and Brooks M S S 1989 *J. Phys.: Condens. Matter* **l** 4005
[81] Norman M R 1990 *Phys. Rev. Lett.* **64** 1162
[82] Norman M R 1991 *Phys. Rev. B* **44** 1364
[83] Terakura K, Oguchi T, Williams A R and Kübler J 1984 *Phys. Rev. B* **30** 4734
[84] Solovyev I V 2005 *Phys. Rev. Lett.* **95** 267205